Dentomaxillofacial Radiology (2014) 43, 20130324

http://birpublications.org/dmfr

RESEARCH ARTICLE

Cross gender–age trabecular texture analysis in cone beam CT

[1]H Ling, [1]X Yang, [1]P Li, [1]V Megalooikonomou, [2]Y Xu and [3]J Yang

[1]Department of Computer and Information Sciences, Temple University, Philadelphia, PA, USA; [2]School of Computer Science and Engineering, South China University of Technology, Guangzhou, China; [3]Division of Oral and Maxillofacial Radiology, Temple University School of Dentistry, Philadelphia, PA, USA

Objectives: To investigate whether multiple texture features in different regions of interest (ROIs) on cone beam CT (CBCT) are correlated with gender–age variation of trabecular patterns.
Methods: CBCT volumes from 96 subjects were used. The data set was divided into four gender–age subgroups, including males younger than 40 years, males older than 40 years, females younger than 40 years and females older than 40 years. For each volume, cubes containing trabecular patterns at four ROIs in the jaws were manually cropped. 18 distinct texture features were calculated and their correlation with gender–age variations at different ROIs was studied through *t*-test statistical analysis.
Results: For the 432 test pairs with different gender–age groups at different ROIs and texture features tested, 149 of them were shown to be statistically different at the 0.05 significance level and 60 of them at the 0.001 significance level. These features can therefore capture changes in trabecular patterns and have the potential to be used for trabecular analysis. Furthermore, fractal features were found to be better than intensity features in separating different gender–age groups. Trabecular patterns in the body of the mandible were more correlated with gender–age changes than other ROIs.
Conclusions: Multiple texture features on CBCT were found to be correlated with the cross gender–age variation of trabecular patterns. The results support the use of CBCT for advanced trabecular analysis, including osteoporosis screening tools in the jaws.
Dentomaxillofacial Radiology (2014) **43,** 20130324. doi: 10.1259/dmfr.20130324

Cite this article as: Ling H, Yang X, Li P, Megalooikonomou V, Xu Y, Yang J. Cross gender–age trabecular texture analysis in cone beam CT. *Dentomaxillofac Radiol* 2014; **43:** 20130324.

Keywords: cone-beam computed tomography; osteoporosis; radiology; fractals; computer-assisted image analysis

Introduction

As a major health problem in the USA, osteoporosis afflicts 55% of Americans aged 50 years and older.[1] Early diagnosis of osteoporosis is very important to prevent more serious complications such as hip fracture. The current gold standard for osteoporosis diagnosis for older patients is based on the bone mineral density measured by dual energy X-ray absorptiometry in the hip and spine region.[2] However, when applied to routine examination for osteoporosis screening, such a gold standard may introduce significant financial burden.

A potential low-cost osteoporosis pre-screening method is through the analysis of dental imaging data, which are collected during routine clinical dental examination at almost no additional cost. In particular, trabecular bone structures in the jaws have been studied for their correlation with bone porosity.[3–7] Despite these studies, it remains an open problem to effectively use dental data for osteoporosis pre-screening. One of the major reasons lies in the inadequacy of using only a limited number of features. In particular, most previous studies have investigated only a few image features [mostly one, often restricted to one region of interest (ROI)], which are not discriminative enough for osteoporosis

Correspondence to: Professor Haibin Ling. E-mail: hbling@temple.edu
Received 30 August 2013; revised 22 January 2014; accepted 28 January 2014

Table 1 Trabecular bone three-dimensional image sample quantity

Group	*Males younger than 40 years*	*Males older than 40 years*	*Females younger than 40 years*	*Females older than 40 years*
Number of volumes	8	27	13	48

pre-screening owing to the large variance and noise in dental data. In fact, many researchers have pointed out the necessity of introducing advanced algorithms to integrate more comprehensive imaging features for dental image-based osteoporosis pre-screening.[5,6,8]

The objective of this study was to investigate multiple texture features and multiple ROIs in cone beam CT (CBCT) that are correlated with the change in trabecular patterns. Based on the fact that trabecular patterns vary across gender and age,[9] it was hypothesized that these features and ROIs provide discriminative information for cross gender–age trabecular analysis in the jaws. Consequently, CBCT volumes from different gender–age groups were used to explore the discriminative power of different texture features.

Methods and materials

Cone beam CT data capture

To evaluate the proposed method, a data set was used which contains 96 anonymized three-dimensional (3D) CBCT volumes from 4 gender–age subgroups, including females younger (FY) than 40 years, females older (FO) than 40 years, males younger (MY) than 40 years and males older (MO) than 40 years. In general, older patients have a high probability to be osteoporotic or to have osteopenia when compared with young patients. In the clinic, it was also found that some female patients showed osteoporotic changes in their forties. Therefore, 40 years of age was used as a cut-off in our experiment. Table 1 gives a summary of the gender–age distribution of the subjects. The data set was obtained from 96 dental implant patients who had no pathology in the jaws. The CBCT scan was obtained by using an i-CAT® machine (Imaging Sciences International, Inc., Hatfield, PA) with 0.3-mm voxel sizes, 14-bit greyscales and 8.9-s scan times. The number of slices in 1 CBCT volume is 327. The project was approved by our institutional review board.

No particular calculation was performed to determine the total number of samples, and all 96 volumes in the original collection were used. The differences between the sample sizes of the groups were taken into account when performing statistical analysis. In particular, the sample sizes were used in the *t*-tests.

For each volume, a dentist manually cropped eight cubes from eight different locations in the jaws, including areas apical to the maxillary left and right premolars, mandibular left and right lateral incisors and first molars, and left and right condyles. Each cube was a volume of $19 \times 19 \times 19$ voxels containing trabecular structures of size $5.7 \times 5.7 \times 5.7\,\mathrm{mm}^3$. The size was chosen to maximally enclose a trabecular pattern while containing little non-trabecular material. Some example cubes in the data set are shown in Figure 1. In the rest of the paper, such cubes are called trabecular cubes. Considering the left–right symmetry, the eight locations were grouped into four ROIs, including ROI 1 (the maxillary premolars), ROI 2 (the mandibular first molars), ROI 3 (the mandibular lateral incisors) and ROI 4 (the left and right condyles). The left–right symmetry was not calculated, and the group of left–right ROIs increased the samples in the statistical analysis.

Texture features

First, the set of collected trabecular cubes was defined as $P=\{p_1, p_2, \ldots, p_N\}$, where $N = 768 = 96 \times 8$ is the number of trabecular cubes cropped from the 96 dental CBCT volumes. Each cube $p \in P$ has $19\times19\times19$ voxels and $p\,(i, j, k)$ indicates the CBCT intensity of the (i, j, k)-th voxel in $p, 1 \leq i, j, k \leq 19$. In this article, the following texture features were explored.

1. *Mean intensity* $\mu(p)$: the mean intensity of a cube p was defined as

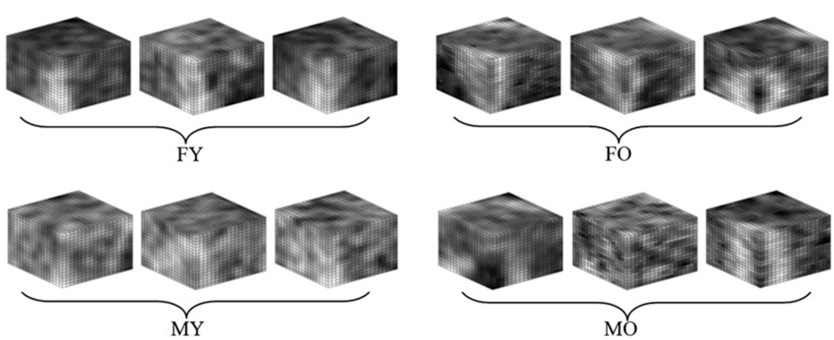

Figure 1 Example trabecular cone beam CT cubes cropped from left condyles in our study. FO, female older than 40 years; FY, female younger than 40 years; MO, male older than 40 years; MY, male younger than 40 years.

$$\mu(p) = \frac{1}{M}\sum_{i=1}^{19}\sum_{j=1}^{19}\sum_{k=1}^{19} p(i,j,k)$$

where $M = 6859 = 19 \times 19 \times 19$ is the number of voxels in a cube.

2. *Intensity histogram* $h(p) = (h_1(p), h_2(p), ..., h_8(p))$: the intensity histogram captures the intensity distribution within a trabecular cube p and therefore provides much richer information than the simple mean intensity. Because of its strong descriptive power, the intensity histogram has been recently popularly used in image processing and pattern recognition for image and texture description.[10,11] In this study, eight intensity bins were defined as $(\tau_m, \tau_{m+1}] : m = 1, ..., 8$, such that τ_1 and τ_9 indicate, respectively, the lower and upper bounds of intensities in the cube p as below

$$\tau_1 = \min_{1 \le i,j,k \le 19} p(i,j,k) - 1$$
$$\tau_9 = \max_{1 \le i,j,k \le 19} p(i,j,k)$$

$\tau_{m+1} = \tau_m + (\tau_9 - \tau_1)/8$ for $m = 1, ..., 7$. Then, the m-th component of the intensity histogram of the cube p was defined as

$$h_m(p) = \#(\{(i,j,k) : \tau_m < p(i,j,k) \le \tau_{m+1}\})$$

where "#" indicates the cardinality of a set. More specifically, $h_m(p)$ was the number of voxels whose intensities fell in the range $(\tau_m, \tau_{m+1}]$. Eight bins were used mainly for two reasons. First, by using eight bins, each bin received an average of about 857 (approximately 6859/8) voxels, which were sufficiently large for constructing statistically meaningful histograms. Second, very large numbers of bins were not used since they might be sensitive to intensity noises and histogram quantization problems, which have been observed in the field of pattern recognition and image analysis.[12]

3. *Fractal dimension* (FD) $\psi(p)$: FD has been used to capture trabecular texture information.[4,13–15] For a trabecular cube p, a 3D point set was first created as $\Lambda = \{(i,j,k) : p(i,j,k) > \tau\}$, where $\tau = \tau_1 + 0.24 \times (\tau_9 - \tau_1)$ was the threshold to filter out irrelevant background voxels in p. The constant number 0.24 was determined according to the visual inspection. More specifically, the threshold helped to discard the majority of background voxels and therefore allowed the FD to focus on trabecular voxels. In other words, when using this threshold, the point set Λ contained most of the trabecular voxels and ignores the majority of background voxels. Then $\psi(p)$ was calculated as the FD of set Λ using the box-counting approach.[16] Specifically, let the 3D Euclidean space be covered by a mesh of 3D cubes with side length r (*i.e.* r-mesh) and a counting function $c(\Lambda, r)$ was defined as the number of r-mesh hypercubes that intersect Λ. Then, the box-counting FD $\psi(p)$ was defined as

$$\psi(p) = \lim_{r \to 0} \frac{\log c(\Lambda, r)}{-\log r}$$

In practice, to approximate the process of $r \to 0$, the slope of $\log(c(\Lambda, r))$ was estimated for a decreasing side-length sequence, $r = 16, 8, 4, 2$ (such that $\log r = 4, 3, 2, 1$), using the least squares method.

4. *Multifractal spectrum* $\phi(p) = (\phi_1(p), \phi_2(p), ..., \phi_8(p))$: owing to the complexity of trabecular patterns, it may be insufficient to describe them using a single FD. Multiple-fractal spectrum is a natural extension to overcome this limitation.[17,18] A cube p was first partitioned into eight disjoint point sets $\{\Lambda_1, \Lambda_2, ..., \Lambda_8\}$ such that

$$\Lambda_m = \{(i,j,k) : \tau_m < p(i,j,k) \le \tau_{m+1}\}, \quad m = 1, 2, ..., 8$$

Then, the m-th element $\phi_m(p)$ was defined as the FD of Λ_m calculated by the box-counting method described above. Eight disjoint sets were used for the same reasons as eight bins were used for the intensity histogram. The partition procedure provides a multiple-fractal spectrum with robustness against common pattern deformations, such as rotation and scaling, since the multiple-fractal spectrum is known to be invariant under the bi-Lipschitz transformation,[17] which subsumes rotation and scaling.

Statistical methods

Statistical analysis on the calculated features is needed to study their effect on separating gender–age groups. One approach is to study the variances and covariances of these features among all four gender–age groups through ANOVA. More specifically, for a given feature, the null hypothesis is that the feature generates the same sample mean for all four groups. However, since the long-term purpose of the study was to prepare guidance for feature selection in future statistical prediction tools, more interest was shown in finding features that can separate two gender–age groups. Consequently, two-sample *t*-test was more suitable, which is in fact a special case of ANOVA in that only two groups of samples are involved.[19]

The two-sample *t*-test was used to study the effects of gender–age on the calculated features. Since there were four gender–age groups in the study, six group pairs were created for comparison: (FO, FY), (FO, MO), (FO, MY), (FY, MO), (FY, MY) and (MO, MY). For each gender–age pair, a statistical analysis for each texture feature (out of 18) on each ROI (out of 4) was conducted. As a result, there were, in total, 432 = 6 × 4 × 18 gender–age test pairs on different ROIs and features, as summarised in Table 2.

For each of the 432 test pairs described above, the two-sample *t*-test was performed to compare them with the null hypothesis and alternative hypothesis (H_A) stated below:

Table 2 *p*-values of all gender–age pairs over different regions of interest (ROIs) and features

		Intensity features									*Fractal dimension features*								
Gender–age pairs	*ROI*	μ	h_1	h_2	h_3	h_4	h_5	h_6	h_7	h_8	ψ	φ_1	φ_2	φ_3	φ_4	φ_5	φ_6	φ_7	φ_8
FO *vs* FY	1	0.065	**0.011**	0.240	0.704	**0.050**	**0.028**	0.090	0.234	0.524	0.105	**0.012**	**0.047**	0.926	0.097	**<0.001**	**<0.001**	0.065	0.279
	2	**<0.001**	**<0.001**	0.104	**<0.001**	**<0.001**	0.576	**<0.001**	**<0.001**	**<0.001**	**<0.001**	0.059	**<0.001**	**<0.001**	**<0.001**	**<0.001**	**<0.001**	**0.023**	**<0.001**
	3	**<0.001**	**0.011**	**0.012**	0.480	0.323	0.744	0.202	0.599	**0.039**	**<0.001**	**<0.001**	0.249	**<0.001**	**<0.001**	**<0.001**	**<0.001**	**0.003**	**<0.001**
	4	0.097	**0.002**	**0.001**	0.070	**0.007**	0.676	**0.001**	**0.016**	0.053	0.163	0.260	0.369	0.133	0.215	0.119	0.054	0.182	0.609
FO *vs* MO	1	0.710	**0.001**	0.069	**0.033**	0.175	0.600	0.208	0.439	0.829	0.350	0.740	0.078	0.060	0.958	0.160	0.059	0.248	0.285
	2	0.261	**0.004**	0.603	0.058	0.340	0.583	0.552	0.342	0.610	**0.010**	0.770	0.206	0.127	0.132	0.262	0.887	0.754	0.107
	3	0.092	**0.015**	0.824	**0.010**	0.183	0.493	**0.006**	0.193	0.667	**0.046**	0.096	**0.041**	0.118	0.926	0.466	**0.040**	0.260	**0.043**
	4	**0.002**	0.654	0.205	0.103	0.244	0.375	0.134	0.100	0.388	0.354	**<0.001**	**0.017**	0.986	0.629	**0.013**	**0.008**	**0.036**	0.413
FO *vs* MY	1	0.238	**0.002**	0.108	**<0.001**	**0.004**	0.092	0.477	0.804	0.516	0.467	0.854	**0.003**	**0.026**	0.773	0.206	0.396	0.714	**0.044**
	2	0.235	0.136	0.507	0.390	0.258	0.564	**0.031**	**0.025**	**0.024**	**0.018**	0.735	0.220	0.412	0.380	0.335	**0.048**	**0.017**	**0.021**
	3	0.736	0.358	0.621	**<0.001**	**0.007**	0.962	0.881	0.947	0.998	0.514	0.075	**0.015**	0.339	0.169	**<0.001**	**<0.001**	0.070	**<0.001**
	4	0.421	0.878	0.238	0.231	0.092	0.054	0.550	0.202	0.309	0.866	0.539	0.056	0.461	0.102	0.145	0.152	0.221	0.503
FY *vs* MO	1	**0.040**	0.71	0.824	0.156	0.718	**0.014**	**0.010**	0.097	0.431	**0.024**	**0.031**	0.555	0.205	0.139	**0.015**	**0.009**	0.344	0.918
	2	**<0.001**	**<0.001**	0.058	**<0.001**	**<0.001**	0.262	**<0.001**	**<0.001**	**<0.001**	**<0.001**	**0.045**	**<0.001**	**<0.001**	**<0.001**	**<0.001**	**<0.001**	0.076	**<0.001**
	3	**<0.001**	**<0.001**	**0.018**	**0.007**	**0.050**	0.896	0.410	0.149	**0.030**	**<0.001**	**<0.001**	**0.013**	**<0.001**	**<0.001**	**0.002**	**0.020**	0.290	**0.001**
	4	**0.007**	**0.035**	**<0.001**	0.874	0.329	0.781	**0.046**	0.112	0.250	0.932	**0.003**	0.312	0.174	0.142	**0.002**	**<0.001**	**0.008**	0.228
FY *vs* MY	1	**0.012**	0.501	0.622	**0.003**	0.258	0.621	0.127	0.270	0.332	**0.047**	0.084	0.270	0.083	0.361	0.198	0.063	0.277	0.292
	2	0.131	0.108	0.396	0.064	**0.019**	0.329	0.758	0.057	**0.043**	0.128	0.088	**0.040**	0.095	0.079	0.071	0.138	0.655	0.539
	3	**0.001**	**0.006**	0.109	**<0.001**	**0.002**	0.756	0.382	0.602	0.088	**0.040**	0.216	**0.005**	**0.002**	**0.028**	0.163	0.201	0.404	0.109
	4	0.058	0.053	**0.006**	0.753	**0.001**	0.191	0.060	0.324	0.684	0.221	0.215	0.302	0.087	**0.029**	**0.025**	**0.026**	0.053	0.321
MO *vs* MY	1	0.404	0.725	0.732	**0.028**	0.171	**0.046**	0.940	0.714	0.595	0.982	0.967	0.072	0.456	0.812	0.737	0.720	0.700	0.230
	2	0.080	**0.005**	0.317	0.091	0.105	0.825	**0.013**	**0.007**	**0.014**	**<0.001**	0.902	0.052	0.105	0.080	0.100	**0.042**	0.052	0.151
	3	0.261	0.283	0.528	0.351	0.146	0.597	0.079	0.286	0.778	0.081	**0.006**	0.467	0.867	0.199	**0.039**	0.176	0.713	0.074
	4	0.463	0.690	0.637	0.670	**0.034**	0.240	0.686	0.700	0.643	0.367	0.351	0.839	0.520	0.178	0.410	0.205	0.336	0.995

FO, females older than 40 years; FY, females younger than 40 years; MO, males older than 40 years; MY, males younger than 40 years.
The four ROIs are ROI 1 for maxillary premolar, ROI 2 for mandibular first premolar, ROI 3 for mandibular lateral incisor and ROI 4 for mandibular condyle. Bold values indicate significance.

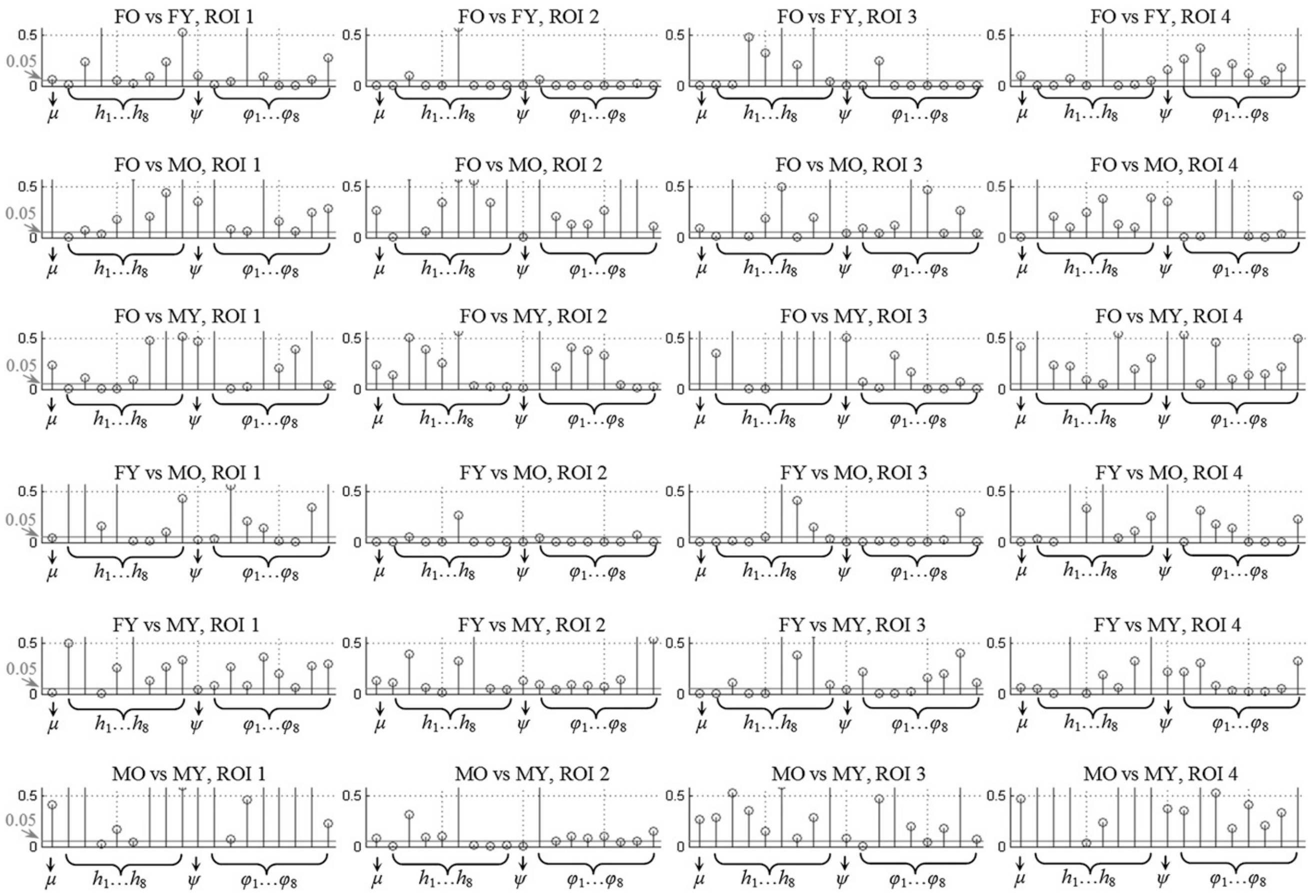

Figure 2 *p*-values of all gender–age pairs over different regions of interest (ROIs) and features. FO, female older than 40 years; FY, female younger than 40 years; MO, male older than 40 years; MY, male younger than 40 years.

H_0: data in the two categories are from normal distributions with equal means.

H_A: data in the two categories are from normal distributions with different means.

The test statistic t was defined as

$$t = \frac{(\mu_1 - \mu_2)}{\sqrt{S^2(1/n_1 + 1/n_2)}}$$

where μ_1 and μ_2 are the sample means of the two categories under comparison; n_1 and n_2 are the numbers of samples in the two categories; and S^2 was defined as

$$S^2 = \frac{(n_1 - 1)S_1^2 + (n_2 - 1)S_2^2}{n_1 + n_2 - 2}$$

where S_1^2 and S_2^2 are the sample variances of the two categories, respectively. Finally, the *p*-value of the *t*-test was calculated from the test statistic with respect to the degrees of freedom $d = n_1 + n_2 - 2$.

Results

The *p*-values of the *t*-tests on all gender–age pairs at different ROIs with different features are reported in

Table 3 The effectiveness of different features

	Intensity features									*Fractal dimension features*								
Feature	μ	h_1	h_2	h_3	h_4	h_5	h_6	h_7	h_8	ψ	ϕ_1	ϕ_2	ϕ_3	ϕ_4	ϕ_5	ϕ_6	ϕ_7	ϕ_8
NoT	9.0	13.0	5.0	10.0	11.0	3.0	8.0	5.0	7.0	11.0	8.0	10.0	6.0	6.0	11.0	13.0	5.0	8.0
PoT	37.5	54.2	20.8	41.7	45.8	12.5	33.3	20.8	29.2	45.8	33.3	41.7	25.0	25.0	45.8	54.2	20.8	33.3
Feature	μ	h_1	h_2	h_3	h_4	h_5	h_6	h_7	h_8	ψ	ϕ_1	ϕ_2	ϕ_3	ϕ_4	ϕ_5	ϕ_6	ϕ_7	ϕ_8
Mean PoT	32.9 ± 13.4									36.1 ± 11.4								

NoT, number of tests in which a feature significantly ($p \leq 0.05$) distinguishes two categories. For example, in the first column of the first row; NoT = 9 means that (as shown in bold in the first column of Table 2) 9 out of the 24 *p*-values corresponding to μ are ≤0.05; PoT, percentage of tests, which was defined as PoT = NoT/24.

Table 4 Number of effective features for each gender–age pair and regions of interest (ROIs)

ROI	*FO* vs *FY*	*FO* vs *MO*	*FO* vs *MY*	*FY* vs *MO*	*FY* vs *MY*	*MO* vs *MY*
1	7.00	2.00	6.00	7.0	3.00	2.00
2	15.00	2.00	7.00	15.0	3.00	6.00
3	12.00	7.00	6.00	14.0	8.00	2.00
4	5.00	6.00	0	8.0	5.00	1.00
Mean	9.75	4.25	4.75	11.0	4.75	2.75

FO, females older than 40 years; FY, females younger than 40 years; MO, males older than 40 years; MY, male younger than 40 years.
Data are the number of features (out of a total of 18) that are effective in the tests involving corresponding gender–age pairs and ROIs. For example, in the first column of the first row, 7 means that (as shown in bold in the first row of Table 2) 7 out of the 18 p-values corresponding to (FO, FY) in ROI 1 are ≤ 0.05.

Table 2. The results with $p \leq 0.05$ are highlighted in the table. In addition, all these p-values are plotted in Figure 2 for better illustration. From these results, it could be observed that many of the tested features (149 out of 432) were correlated significantly with the gender–age variation at the 0.05 level, with some of them (60 out of 432) at the 0.001 level.

The effectiveness of different features, ROIs and gender–age pairs in capturing the cross gender–age trabecular variations was also studied. First, for the effectiveness of a specific feature, the times it correlated significantly ($p = 0.05$) with different gender–age groups at different ROIs were counted. These numbers are summarised in Table 3. The average effectiveness of the two groups of features, *i.e.* intensity features and FD features, was also calculated. Second, the numbers of effective features for each gender–age pair and ROI are summarized in Table 4. The results illustrate how the proposed features in general were correlated with the variation of trabecular patterns across different gender–age groups at different ROIs.

Discussion

Variations in trabecular bone patterns have been known to reflect bone density change, which suggests the potential of analysing trabecular patterns for pre-screening bone diseases such as osteoporosis. In the past few decades, trabecular bone structure analysis has been studied in various biomedical contexts. The importance of trabecular perforations in the development of osteoporosis had been introduced by Parfitt et al.[20] Previous research has also explained the relation between the profound disintegration of the trabecular bone network and certain bone disease.[21,22] Moreover, studies have shown that changes in the iliac trabecular bone texture can predict osteoporosis by means of changes in surface texture, volume and thickness.[22]

This study was highly motivated by a series of investigations looking at a potential low-cost osteoporosis pre-screening method using dental imaging data.[3–7] The widely used dental panoramic radiography is cost-effective since it is often a by-product of routine dental examination. In particular, trabecular bone structures in the jaws have been studied for their correlation with bone porosity. White and Rudolph[6] showed that the trabecular patterns of osteoporosis patients are altered compared with those of normal subjects. White[5] used FD to analyse the trabecular bone structure in relation to osteoporosis. Southard et al[4] showed that the radiographic FD of the alveolar process bone is correlated with the bone density, using radiographic images. Pham et al[3] found that panoramic radiographs can be used for assessment of trabecular bone patterns with the aid of a visual index. Yang et al[7] found that oestrogen deficiency can result in microarchitectural alterations of trabecular bone in both the mandible and the tibia.

Recently, there has been a trend to include CBCT in 3D dental examinations.[23] Consequently, it is of interest to study how the trabecular patterns in CBCT correlate with bone porosity. Although a correlation between the dental trabecular pattern and osteoporosis has been discovered using dental panoramic radiography and CT,[8,24] such a correlation is not directly available in dental CBCT. One reason lies in that dental CBCT usually has a low resolution (*e.g.* 0.3–0.4 mm), which causes serious blur in trabecular structures, which are typically around 0.1 mm in bone thickness. Furthermore, because of the distortion of CBCT measurement from dental CT values, there has been a debate on whether CBCT measurement can be used to infer bone mineral densities.[21,25–27]

Despite the large number of studies showing the positive correlation of texture features with changes in trabecular patterns, there is still some way to go before trabecular analysis can be used for osteoporosis pre-screening. Advanced image analysis and statistical learning tools have been expected to be used to address this issue.[5] On the other hand, there has been great progress in the field of texture analysis and machine learning, as well as their application to medical image analysis tasks.

In previous studies,[4,6,13–15] only basic texture descriptors, such as intensity and Fourier analysis, have been used to confirm the correlation between the loss of bone mass and the trabecular patterns. It has also been observed that these features by themselves are insufficient to be used for clinical diagnosis or pre-screening purposes. A potential way to address this issue is to exploit multiple texture descriptors and combine them together with advanced statistical learning tools. The focus of this article is the first step towards investigating various high-dimensional texture features, including both classical texture descriptors and recently proposed ones.

The results of this study have moved these investigations one step further in this direction. It has demonstrated a series of texture features at four different ROIs for capturing variations in trabecular patterns in dental CBCT. This observation validated the hypothesis that CBCT volumes can be used for cross gender–age analysis of trabecular patterns in the jaws. The results also showed that (1) fractal analysis-based features work generally better than intensity features, (2) FO *vs* FY and FY *vs* MO have significantly more effective features than other pairs, which can be attributed to the loss of bone mass in older females, (3) trabecular patterns in the body of the mandible are more correlated with gender–age changes than those in the maxilla and the mandibular condyles and (4) the mean intensity is less effective than several FD features and several components in the intensity histogram, which may be the result of instability in the CBCT intensity.[21,27]

The results also supported the use of CBCT for the analysis of bone mineral density. Although the detailed trabecular structure is unavailable because of the low resolution used in clinical data, the texture pattern in CBCT still carries useful information reflecting statistics of trabecular patterns, such as the density and regularity of the bone structures. Furthermore, although the CBCT measurement may be distorted from the CT values, some structure-relevant features (*e.g.* those based on fractal analysis) can still provide discriminative information for separating different trabecular patterns.

In summary, the experiment results validated that the cross gender–age variation of trabecular patterns correlates significantly with many texture features on CBCT. It is highly desirable that the imaging tests used in dentistry are fully exploited to generate the maximum diagnostic information related to systemic conditions such as osteoporosis. The results also showed that the rich texture descriptors such as intensity histograms and the multifractal spectrum can provide complementary or more discriminative information than the previously proposed simple texture descriptors.

In the future, it is expected that these features will be combined together, using modern machine learning tools, such as ensemble learning[28] or kernel learning,[29] to predict the loss of bone mass. Such a predictor will in turn provide the basis of dental image-based osteoporosis prescreening.

References

1. National Osteoporosis Foundation. *America's bone health: the state of osteoporosis and low bone mass in our nation*. Washington, DC: National Osteoporosis Foundation; 2002.
2. Kanis JA, Glüer CC. An update on the diagnosis and assessment of osteoporosis with densitometry. Committee of Scientific Advisors, International Osteoporosis Foundation. *Osteoporos Int* 2000; **11**: 192–202.
3. Pham D, Jonasson G, Kiliaridis S. Assessment of trabecular pattern on periapical and panoramic radiographs: a pilot study. *Acta Odontol Scand* 2010; **68**: 91–7. doi: 10.3109/00016350903468235
4. Southard TE, Southard KA, Lee A. Alveolar process fractal dimension and postcranial bone density. *Oral Surg Oral Med Oral Pathol Oral Radiol Endod* 2001; **91**: 486–91. doi: 10.1067/moe.2001.112598
5. White SC. Oral radiographic predictors of osteoporosis. *Dentomaxillofac Radiol* 2002; **31**: 84–92. doi: 10.1038/sj.dmfr.4600674
6. White SC, Rudolph DJ. Alterations of the trabecular pattern of the jaws in patients with osteoporosis. *Oral Surg Oral Med Oral Pathol Oral Radiol Endod* 1999; **88**: 628–35.
7. Yang J, Pham SM, Crabbe DL. High-resolution micro-CT evaluation of mid- to long-term effects of oestrogen deficiency on rat trabecular bone. *Acad Radiol* 2003; **10**: 1153–8.
8. Devlin H, Horner K. Diagnosis of osteoporosis in oral health care. *J Oral Rehabil* 2008; **35**: 152–7. doi: 10.1111/j.1365-2842.2007.01791.x
9. Parfitt AM. Age-related structural changes in trabecular and cortical bone: cellular mechanisms and biomechanical consequences. *Calcif Tissue Int* 1984; **36**(Suppl. 1): S123–8.
10. Jager F, Hornegger J. Nonrigid registration of joint histograms for intensity standardization in magnetic resonance imaging. *IEEE Trans Med Imaging* 2009; **28**: 137–50. doi: 10.1109/TMI.2008.2004429
11. Han JH, Yang S, Lee BU. A novel 3-D color histogram equalization method with uniform 1-D gray scale histogram. *IEEE Trans Image Process* 2011; **20**: 506–12. doi: 10.1109/TIP.2010.2068555
12. Rubner Y, Puzicha J, Tomasi C, Buhmann JM. Empirical evaluation of dissimilarity measures for color and texture. *Comput Vis Image Underst* 2001; **84**: 25–43.
13. Law AN, Bollen AM, Chen SK. Detecting osteoporosis using dental radiographs: a comparison of four methods. *J Am Dent Assoc* 1996; **127**: 1734–42.
14. Ruttimann UE, Webber RL, Hazelrig JB. Fractal dimension from radiographs of peridental alveolar bone. A possible diagnostic indicator of osteoporosis. *Oral Surg Oral Med Oral Pathol* 1992; **74**: 98–110.
15. Yi WJ, Heo MS, Lee SS, Choi SC, Huh KH, Lee SP. Direct measurement of trabecular bone anisotropy using directional fractal dimension and principal axes of inertia. *Oral Surg Oral Med Oral Pathol Oral Radiol Endod* 2007; **104**: 110–16. doi: 10.1016/j.tripleo.2006.11.005
16. Falconer K. *Techniques in fractal geometry*. Chichester, UK: John Wiley & Sons; 1997.
17. Xu Y, Ji H, Fermuller C. Viewpoint invariant texture description using fractal analysis. *Int J Comput Vis* 2009; **83**: 85–100.
18. Ji H, Yang X, Ling H, Xu Y. Wavelet domain multifractal analysis for static and dynamic texture classification. *IEEE Trans Image Process* 2013; **22**: 286–99. doi: 10.1109/TIP.2012.2214040
19. Keller G. *Statistics for management and economics*. Mason, OH: Thomson South-Western; 2008.
20. Parfitt AM, Mathews CH, Villanueva AR, Kleerekoper M, Frame B, Rao DS. Relationships between surface, volume, and thickness of iliac trabecular bone in aging and in osteoporosis. Implications for the microanatomic and cellular mechanisms of bone loss. *J Clin Invest* 1983; **72**: 1396–409. doi: 10.1172/JCI111096
21. Nomura Y, Watanabe H, Honda E, Kurabayashi T. Reliability of voxel values from cone-beam computed tomography for dental use in evaluating bone mineral density. *Clin Oral Implants Res* 2010; **21**: 558–62.
22. Eriksen EF. Normal and pathological remodeling of human trabecular bone: three dimensional reconstruction of the remodeling sequence in normals and in metabolic bone disease. *Endocr Rev* 1986; **7**: 379–408. doi: 10.1210/edrv-7-4-379

23. Alamri HM, Sadrameli M, Alshalhoob MA, Sadrameli M, Alshehri MA. Applications of CBCT in dental practice: a review of the literature. *Gen Dent* 2012; **60**: 390–400.
24. Ardakani FE, Mirmohamadi SJ. Osteoporosis and oral bone resorption: a review. *J Maxillofac Oral Surg* 2009; **8**: 121–6. doi: 10.1007/s12663-009-0030-y
25. Hua Y, Nackaerts O, Duyck J, Maes F, Jacobs R. Bone quality assessment based on cone beam computed tomography imaging. *Clin Oral Implants Res* 2009; **20**: 767–71. doi: 10.1111/j.1600-0501.2008.01677.x
26. Katsumata A, Hirukawa A, Noujeim M, Okumura S, Naitoh M, Fujishita M, et al. Image artifact in dental cone-beam CT. *Oral Surg Oral Med Oral Pathol Oral Radiol Endod* 2006; **101**: 652–7. doi: 10.1016/j.tripleo.2005.07.027
27. Lee S, Gantes B, Riggs M, Crigger M. Bone density assessments of dental implant sites: 3. Bone quality evaluation during osteotomy and implant placement. *Int J Oral Maxillofac Implants* 2007; **22**: 208–12.
28. Breiman L. Random forests. *Mach Learn* 2001; **45**: 5–32.
29. Vapnik V. *The nature of statistical learning theory*. New York, NY: Springer-Verlag; 1995.